Revealing the Catalytic Role of Sn Dopant in CO_2-Oxidative Dehydrogenation of Propane over Pt/Sn-CeO_2 Catalyst

Yehong Wang[a, b*], Jiapei Wang [a], Yuda Zhang [a], (Dr.) Qiang Guo [a], Jie An [a], Yafei Liang [a], Yanan Wang [a], (Dr.) Pengfei Cao[c], (Prof. Dr) Marc Heggen[c], (Prof. Dr.) Rafal E. Dunin-Borkowski[c], (Prof. Dr.) Xiangxue Zhu [a], (Prof. Dr.) Xiujie Li [a*], (Prof. Dr.) Feng Wang [a]

a. Dalian National Laboratory for Clean Energy, Dalian Institute of Chemical Physics, Chinese Academy of Sciences, 457 Zhongshan Road, Dalian 116023, China

b. University of Chinese Academy of Sciences, Beijing 100049, China

c. Ernst Ruska Centre for Microscopy and Spectroscopy with Electrons and Peter Grünberg Institute, Forschungszentrum Juelich GmbH, Juelich 52425, Germany

*Corresponding author: Yehong Wang, wangyehong@dicp.ac.cn; Xiujie Li, xiujieli@dicp.ac.cn

Abstract

CO_2-oxidative dehydrogenation of propane (CO_2-ODHP) provides a promising route for propylene production. Sufficient propane conversion and propylene selectivity remain a great challenge due to the difficulty in activating inert propane and CO_2 simultaneously. Here, we reported a Sn doped CeO_2 supported Pt (Pt/Sn-CeO_2) catalyst in CO_2-ODHP reaction. Sn doping appears to kill two birds with one stone for propane and CO_2 activation. On the one side, it increases the electron density of Pt species via PtSn alloy formation, promoting propane adsorption and C–H bond cleavage. On the other side, it enhances oxygen vacancy concentrations of CeO_2 support, facilitating CO_2 dissociation. A higher propylene selectivity (63.9% *vs* 22.3%) was obtained on 0.1 wt% Pt/1.0 wt% Sn-CeO_2 than that on 0.1 wt% Pt/CeO_2 with a comparable propane conversion (15.1% *vs* 14.3%) at 550 °C after 240 min on stream. This work provides a reference for designing efficient catalysts.

Introduction

Propylene, as one of the important industrial raw materials, has been widely used as building blocks for the production of various value-added chemicals, such as polypropylene and polyacrylonitrile [1]. Much attention has been paid to the direct dehydrogenation of propane to propylene because of its superior selectivity. However, this endothermic dehydrogenation process suffers from high energy consumption due to the thermodynamically limited process, as well as a rapid deactivation of catalysts from the coke formation [2]. Although the O_2-oxidative dehydrogenation of propane could overcome the abovementioned disadvantages, it generally proceeds along with the excessive oxidation of propane to CO_2 derived from the high oxidizing ability of O_2, decreasing the propylene selectivity [3-5]. Alternatively, CO_2, as a soft oxidant, has been widely used in many reactions [3]. The CO_2-oxidative dehydrogenation of propane (CO_2-ODHP) has been identified as a promising process for propylene production [1, 6, 7]. It is still a great challenge to achieve high propylene selectivity and propane conversion due to the thermodynamical and chemical stability of both propane and CO_2. [8]. Therefore, developing efficient catalysts with excellent catalytic activity in the selective cleavage of C–H bond and CO_2 activation is in a great demand.

Two typical reaction mechanisms of CO_2-ODHP reaction have been reported: 1) MvK mechanism over reducible catalysts (such as CrO_x, and VO_x); and 2) two-step mechanism involved propane dehydrogenation and reverse water-gas shift processes over non-reducible catalysts (such as GaO_x, and InO_x) (Scheme 1) [1,7]. Both of them suggests the necessity for the C–H bond cleavage and CO_2 activation. Supported Pt materials are well-known propane dehydrogenation catalysts, because of their excellent selectivity in C–H bond cleavage accompanying with limited C–C bond cleavage [9]. Nonetheless, introduction of a second metal as a promoter is generally essential and fascinating to further enhance the propylene selectivity and stability of Pt catalysts [10, 11]. In particular, tin, as the most studied promoter so far, shows both geometric and electronic effects on the catalysis of Pt species in the propane dehydrogenation [12, 13]. It not only promotes the dispersion of Pt species, but also modify the electronic

properties of Pt species [2, 14]. When CO_2 was applied as a soft oxidant in the oxidation dehydrogenation of propane, a MvK mechanism is generally involved which is related to a redox process including CO_2 dissociation (**Scheme 1**) [15]. CeO_2, which possesses excellent redox properties, has been considered as an attractive catalyst for CO_2 dissociation [15-22]. Its superior capability derives from the unique oxygen-releasing ability, which is closely linked to its defective structure with oxygen vacancies [23]. Rich oxygen vacancies on CeO_2 will facilitate CO_2 dissociation. Previous work in propane dehydrogenation over ceria supported catalysts primarily focuses on the interaction between Pt and Sn, which were introduced into ceria supports by conventional co-impregnation method [24]. And the effects of Ce as promoter on supported PtSn catalysts were also reported [25, 26]. However, understanding of the interaction among Pt, Sn species and ceria support is still limited. For CeO_2-based catalysts, metal-doping has been used as an efficient way to enhance the formation of oxygen vacancies and it was found that Sn doping significantly improves the oxygen vacancy concentrations of CeO_2 in our previous work [23, 27-30]. Inspired by the direct dehydrogenation property of Pt, CO_2 activation ability of CeO_2, and doping effects of Sn, designing a supported Pt catalysts with Sn doped CeO_2 as support would show a great potential to realize the multiple functions required to activate C–H bonds and inert CO_2 simultaneously in CO_2-ODHP, contributing to the further understanding of the interaction of Pt, Sn metals and ceria supports.

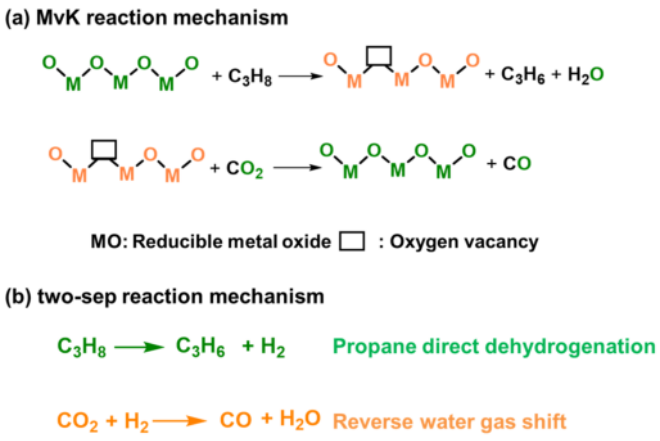

Scheme 1. Reaction mechanism of CO_2-ODHP reaction. (a) MvK reaction mechanism; (b) two-step reaction mechanism.

In this work, a multifunctional Sn doped CeO_2-supported Pt (Pt/Sn-CeO_2) catalyst was prepared, achieving a high propylene selectivity of 63.9% with propane conversion at 15.1% in CO_2-ODHP reaction over 0.1 Pt/1.0Sn-CeO_2 at 550 °C for 240 min. Enhanced selectivity was attributed to the influence of Sn doping on the activation of propane and CO_2. Further characterizations reveal that Sn doping could improve the electron density of Pt species and oxygen vacancy concentration of CeO_2 support simultaneously, resulting in the enhancement of propane adsorption and CO_2 dissociation. At last, a MvK reaction mechanism was proposed on the basis of the *in situ* IR results.

Results and discussion

Catalytic performances of 1.0 Pt/CeO_2 and 1.0 Pt/*n* Sn-CeO_2

1.0 Pt/ *n* Sn-CeO_2 catalysts with various Sn doping amounts (0.5 wt%, 1.0 wt%, 2.0 wt% and 5.0 wt%) were prepared and applied in the CO_2-ODHP reaction at 550 °C. 1.0 Pt/CeO_2 was also prepared and evaluated for comparison. 1.0 Pt/CeO_2 showed 98 % propane conversion which is the highest in the initial 20 min **(Fig. 1a**) and the CO_2-ODHP reaction did not occur without catalysts (**Table S1, entry 1**). Prolonging the reaction time, propane conversion on 1.0 Pt/CeO_2 decreased and maintained at around 70% after reaction for 280 min. Considering the fact that the equilibrium conversion of propane in CO_2-ODHP is 33% under this reaction condition, the transformation of propane and CO_2 over 1.0 Pt/CeO_2 proceeded not only via CO_2-ODHP but also other routes such as dry reforming of propane via C–C bond cleavage, which has a high equilibrium conversion (>99%) under this reaction conditions [35]. Instead of pristine CeO_2 by Sn-CeO_2 as the support, the propane conversion decreased remarkably. The initial propane conversion dropped to 75%~90%, and then continued decreasing to 43%~57% over 1.0 Pt/*n* Sn-CeO_2 catalysts after reaction for 280 min. In addition, the ceria-based catalysts (1.0 Pt/CeO_2 and 1.0 Pt/*n* Sn-CeO_2) exhibited high CO_2 conversions (56-96%), suggesting the excellent ability of these catalysts for CO_2 activation and reduction (**Fig. 1b**). Although the Sn doping decreased the propane conversion, it improved the selectivity of propylene significantly (**Fig. 1c**). The highest

selectivity of propylene was obtained over 1.0 Pt/1.0 Sn-CeO_2 (27.8%), which was higher than that over 1.0 Pt/ CeO_2 (< 2.5%) and other 1.0 Pt/ *n* Sn-CeO_2 catalysts (< 23.9%).

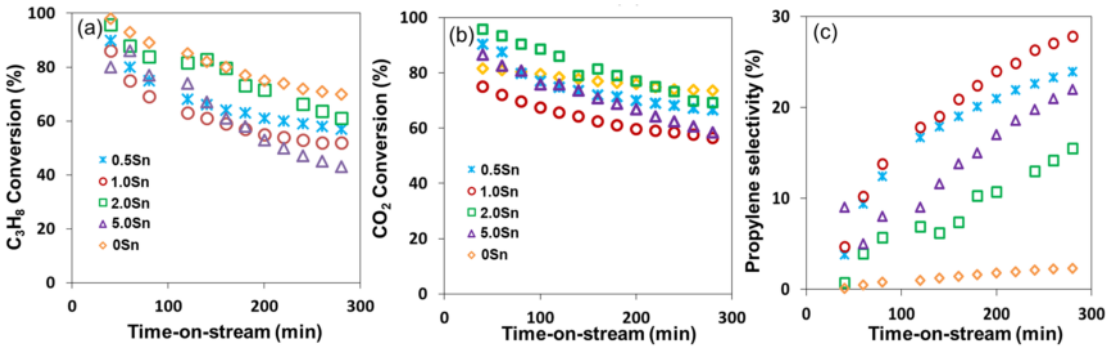

Fig. 1. Catalytic CO_2-ODHP over 1.0 Pt/CeO_2 and 1.0 Pt/*n* Sn-CeO_2 with various Sn doping amounts ranging from 0.5 wt% to 5 wt%. (a) Conversion of propane; (b) conversion of CO_2; (c) propylene selectivity.

The major by-products are CH_4, C_2H_6 and CO, which were produced via cracking and dry reforming processes (**Fig. 2a**). A comparison of catalytic performances over 1.0 Pt/CeO_2 and 1.0 Pt/ *n* Sn-CeO_2 suggested that Sn doping with moderate Sn amounts (1 wt% Sn) contributed to the selective generation of propylene with a comparable propane/CO_2 conversion in the CO_2-ODHP reaction (**Fig. 2b**). Propylene yield was calculated on the basis of propane conversion and propylene selectivity and it increased during the reaction and leveled off after reaction for 200 min over all catalysts (**Fig. S1)**. The highest propylene yield (14.5%) was obtained over 1.0 Pt/1.0 Sn-CeO_2 catalyst. Therefore, 1.0 Sn-CeO_2 was selected as the optimal support for the subsequent investigation.

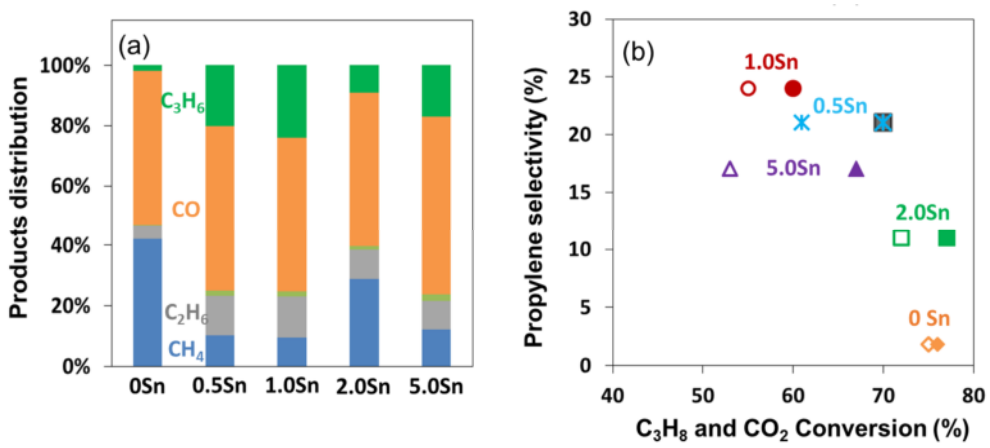

Fig. 2. Catalytic CO_2-ODHP over 1.0 Pt/CeO_2 and 1.0 Pt/*n* Sn-CeO_2 with various Sn doping amounts ranging from 0.5 wt% to 5 wt%; (a) products distribution after reaction for 200 min; (b) the C_3H_8/CO_2 conversion *vs* propylene selectivity after reaction for 200 min. The solid ones represent the CO_2 conversion, while the other ones represent C_3H_8 conversion.

Effects of Sn-doping on Pt chemical states and ceria properties in 1.0 Pt/n Sn-CeO_2

The catalytic performances of supported PtSn catalysts could be regulated by both the geometric effect and electronic effects of Pt species induced by Sn modification. Firstly, the geometric or size effect of Pt species induced by Sn doping was investigated by elemental mapping. Typically, the catalysts of 1.0 Pt/CeO_2, 1.0 Pt/1.0 Sn-CeO_2, and 1.0 Pt/5.0 Sn-CeO_2 were chosen as the representative ones and their results are shown in **Fig. 3**. It shows that most of Pt species were homogeneously distributed over the ceria-based supports, particularly over Sn doped ceria supports. Some bright part was observed from Pt elemental mapping in certain locations, suggesting that part of Pt sites tend to be aggregated. No obvious difference in Pt particle size was observed between 1.0 Pt/1.0 Sn-CeO_2 and 1.0 Pt/5.0 Sn-CeO_2. This indicates that the differences in catalytic performances are not so closely associated with geometric effects of Pt species induced by Sn doping.

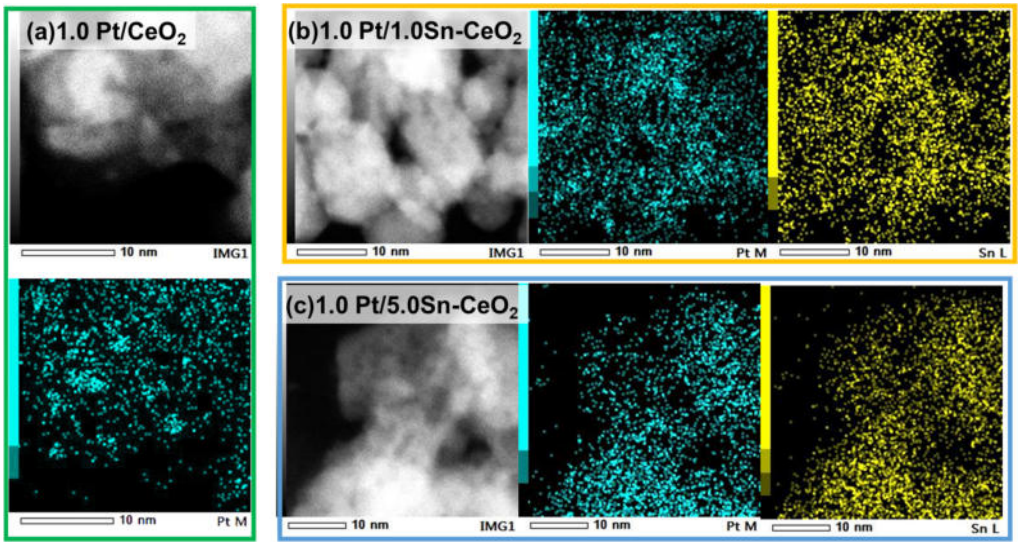

Fig. 3. Elemental mapping results of (a) 1.0 Pt/CeO_2, (b)1.0 Pt/1.0Sn-CeO_2, and (c) 1.0 Pt/5.0 Sn-CeO_2, respectively. Before the detection, these samples were reduced at 450 ^oC for 1 h in H_2 (25 mL/min).

Further study was focused on the chemical states of Pt species induced by Sn doping. The effects of Sn-doping were then studied and XPS was firstly conducted to investigate the effects of Sn doping on the chemical states of Pt species over 1.0 Pt/CeO_2, 1.0 Pt/1.0 Sn-CeO_2, and 1.0 Pt/5.0 Sn-CeO_2, respectively (**Fig. 4**). From the 4f Pt XPS spectra, both positively charged Pt (Pt^{n+}) and metallic Pt (Pt^0) species were observed on all these samples, which verified by the presence of two peaks located at the binding energy of 71.9 eV and 70.85~71.53 eV, respectively [36]. It was known that the Pt^0 species was generally located at a binding energy of 70.5~70.9 eV and would shift to a higher binding energy (71.2~71.5 eV) when it was supported on reducible metal oxides due to the strong metal-support interaction via electron transfer from metal to supports. Here, the binding energy associated with Pt^0 species on1.0 Pt/1.0 Sn-CeO_2 (70.85 eV) is lower than those on 1.0 Pt/CeO_2 (71.53 eV) and 1.0 Pt/5.0 Sn-CeO_2 (71.48 eV) and this demonstrates that Sn doping with moderate Sn amount weakens the interaction between Pt and Sn-CeO_2 support, leading to the formation of Pt^0 species with rich electrons.

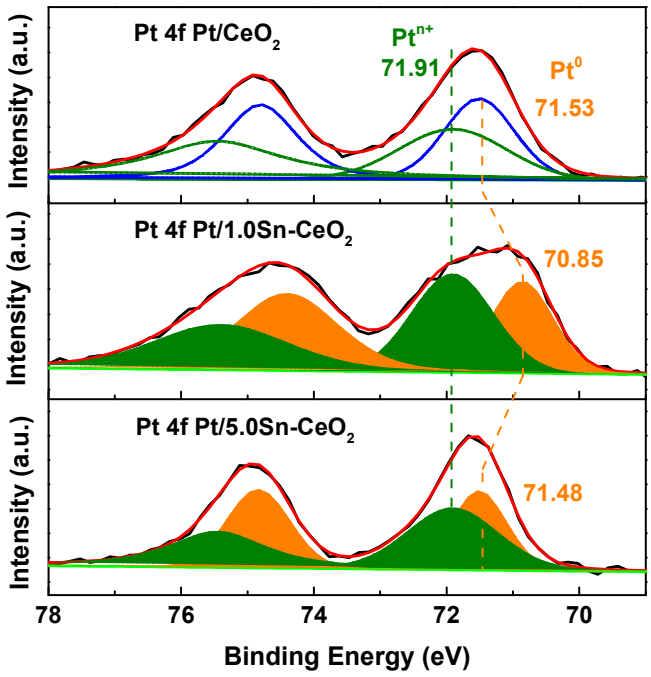

Fig. 4. Pt 4f XPS of 1.0 Pt/CeO_2, 1.0 Pt/1.0 $Sn-CeO_2$, and 1.0 Pt/5.0 $Sn-CeO_2$. These samples were reduced at 450 ºC for 1 h in H_2 before XPS detection.

Fig. 5 shows the 3d Sn spectrum of 1.0Pt/1.0$Sn-CeO_2$ which indicates that the Sn species mainly consists of tin oxide (Sn^{n+}) and metallic Sn (Sn^0), as demonstrated by a BE at 485.5 eV and 486.2 eV, respectively. The formation of Sn^0 along with the formation of electron-rich Pt^0 species reveals the possibility of the formation of alloyed Sn^0 with Pt (PtSn alloy), which is consistent with the reported results [37, 38]. The proportion of Sn^0 species was estimated to be ~26%, while the left ~74% tin species which present as Sn^{n+} was probably anchored into CeO_2 matrix and maintained its oxidation states during the activation via reduction.

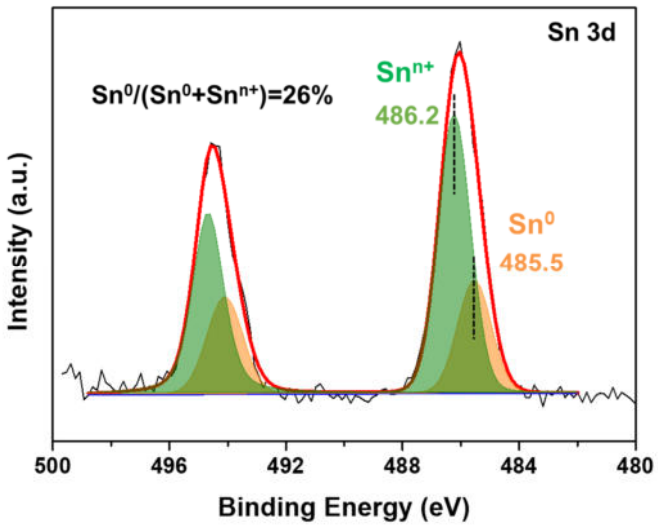

Fig. 5. Sn 3d XPS of 1.0 Pt/1.0 Sn-CeO_2. The sample was reduced at 450 °C for 1 h in H_2 before XPS detection.

The chemical states of Pt species on 1.0 Pt/CeO_2, and 1.0 Pt/*n* Sn-CeO_2 were also studied by FTIR with CO as a probe (**Fig. 6a**). It confirmed the co-existence of Pt^{n+} and Pt^0 sites on these samples, which was consistent with XPS results. For 1.0 Pt/CeO_2, the band located at 2122 cm^{-1} was assigned to the vibration of CO adsorbed on the Pt^{n+} sites, while the bands at 2085 and 2070 cm^{-1} could be attributed to that on Pt^0 sites [36, 39, 40]. With 0.5 wt%~1.0 wt% Sn doping, there was only one major band located at around 2070 cm^{-1}. With increasing the Sn doping amount to 2.0 wt%~5.0 wt%, this band blue-shifted from 2070 cm^{-1} to 2080 cm^{-1} again, suggesting lower electronic density of Pt sites on 2.0 Sn-CeO_2 and 5.0 Sn-CeO_2 [41, 42]. These abovementioned results confirmed the presence of Pt species with rich electrons over 1.0 Pt/1.0 Sn-CeO_2. It was in a good agreement with XPS results. A relationship between the wavenumbers of CO adsorption from CO-IR and the catalytic activity was established (**Fig. 6b**). It indicated that the presence of Pt^0 sites with rich electrons induced by Sn doping might contribute to the superiority of 1.0 Pt/1.0 Sn-CeO_2 in the selective conversion of propane and CO_2.

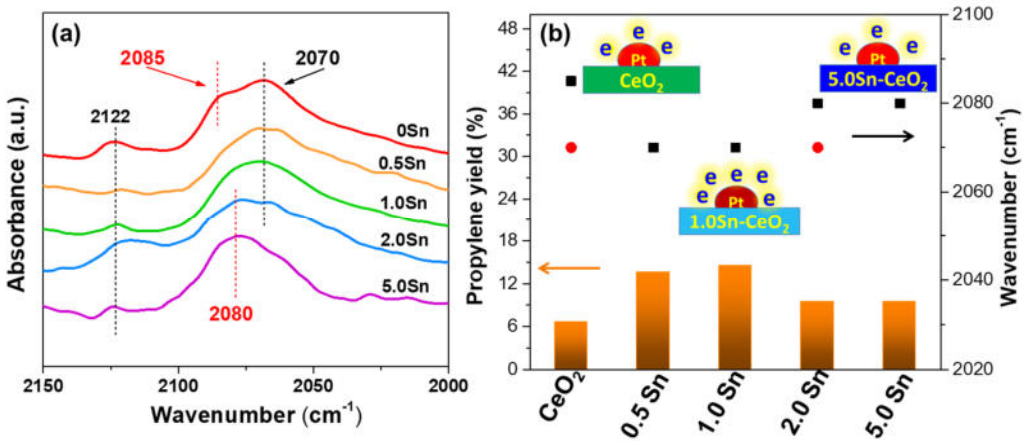

Fig. 6. (a) CO-IR spectra of 1.0 Pt/CeO_2 and 1.0 Pt/*n* Sn-CeO_2 with various Sn doping amounts ranging from 0.5 wt% to 5.0 wt%. These spectra were collected at 30 °C after desorption at 100 °C for 30 min. (b) Relationship between propylene yield and wavenumbers from CO-IR for various 1.0 Pt/Sn-CeO_2 catalysts. The propylene yield is obtained from the reaction for 200 min.

Sn as dopant was introduced into CeO_2 and might affect the structure and defect properties of CeO_2 matrix. Thus, a series of characterizations were performed to investigate the structures of CeO_2-based catalysts before and after Sn doping. From the XRD patterns of pristine CeO_2, the diffraction peaks at 2θ = 28.5°, 33.0°, 47.4°, 56.3° were corresponded to the planes (111), (200), (220) and (311) of CeO_2 fluorite-type structure, respectively [31, 43] (**Fig. S2**). After the Sn doping, no new diffraction peak and remarkable shift was observed, indicating that a low Sn doping amount made it highly dispersed into CeO_2 matrix and exceeded the limit of XRD detection, which was consistent with the elemental mapping results.

Raman spectra showed two obvious bands located at 462 cm^{-1} and 595 cm^{-1} on CeO_2 and 1.0 Sn-CeO_2 (**Fig. 7**), which were assigned to F_{2g} vibration of CeO_2 lattice and vibration associated with oxygen vacancies, respectively [44, 45]. The ratio of peak intensity at 595 cm^{-1} to that at 462 cm^{-1} was calculated to evaluate the concentration of defects [44]. It is 0.02 for pristine CeO_2 and increases with Sn doping. It reached 0.44 when 5 wt% Sn was doped into ceria matrix, indicating the promotion of oxygen vacancies formation on CeO_2 by Sn doping.

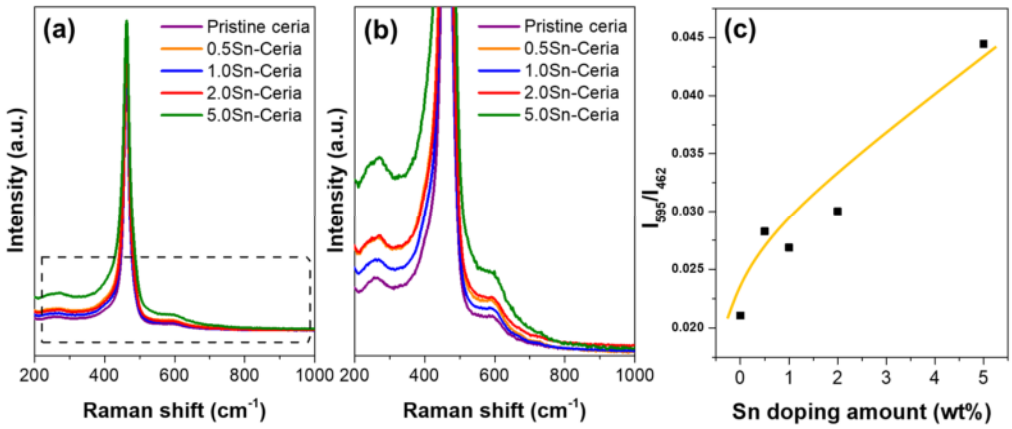

Fig. 7. (a) Raman spectra of CeO_2 and 1.0 Sn-CeO_2 supports. (b) Raman spectra with a magnification of the peak located at around 595 cm^{-1}, which is associated with the formation of oxygen vacancies.

Optimization of Pt loading amounts of *m* Pt/1.0 Sn-CeO_2

Optimization of Pt loading amounts with 1.0 Sn-CeO_2 as the support was performed and a series of Pt loading amounts including 0.1 wt%, 0.3 wt%, 0.5 wt%, 0.8 wt% and 1.0 wt% were investigated. These catalysts were applied in the CO_2-ODHP reaction and the results are shown in **Fig. 8.** With increasing the Pt loading amounts from 0.1 wt% to 0.8 wt%, the propane conversion increased from 15.1% to 79.0%. Continuing to increase it to 1.0 wt%, the propane conversion decreased to 52.0% (**Fig. 8a**). For *m* Pt/1.0 Sn-CeO_2 catalysts, the CO_2 conversion showed similar changing trend as propane conversion. Higher CO_2 conversions than that of propane were observed, indicating the propane activation might be the determination step in the presence of enough oxygen vacancies on ceria-based supports (particularly 1.0 Sn-CeO_2) for CO_2 activation. Although a low Pt loading amount (particularly 0.1 wt% Pt) showed a negative effect on the conversion of propane, it exhibited a high propylene selectivity. It showed a 63.9% propylene selectivity over 0.1 Pt/1.0 Sn-CeO_2 catalyst, which was higher than that that of other catalysts (< 37%) (**Fig. 8b and Table S1, entry 2**).

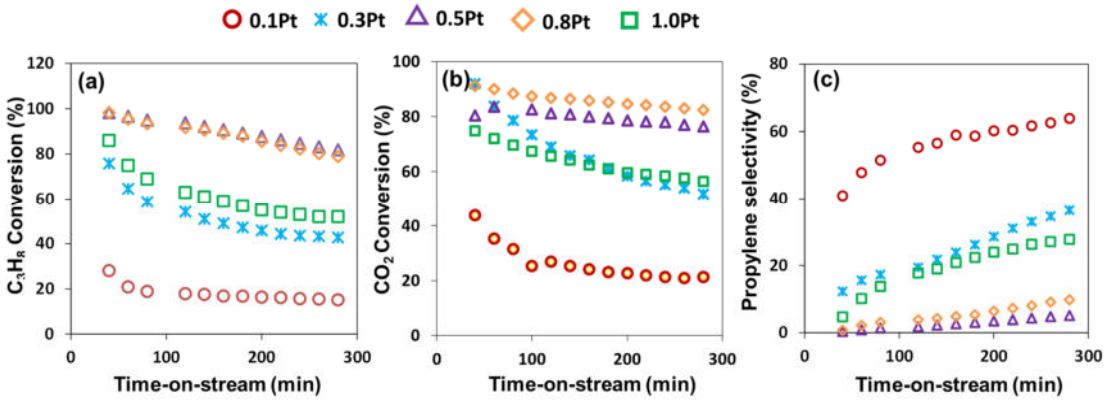

Fig. 8. Catalytic CO_2-ODHP over *m* Pt/1.0 Sn-CeO_2 catalysts with various Pt loading amounts ranging from 0.1 wt% to 1.0 wt%. (a) Conversion of propane; (b) conversion of CO_2; (c) propylene selectivity.

From the products distribution after reaction for 200 min, it indicated that the propylene selectivity decreased from 62.2% to 5.3% with increasing the Pt loading amounts from 0.1 wt% to 0.5 wt%, which was accompanied by the generation of CO and CH_4 as by-products via C–C bond cleavage. With increasing the Pt loading amount to 0.8 wt% and 1.0 wt%, the propylene selectivity was enhanced to 25.5% and 50.1%, respectively, with CO, CH_4, and C_2H_6 as the by-products (**Fig. 9a**). These results showed that 0.1 wt% of Pt loading amount was the optimal one when 1.0 Sn-CeO_2 was applied as the support. For comparison, 0.1 Pt/CeO_2 showed a comparable propane conversion (14.3%), but a lower propylene selectivity (22.3%) (**Table S1, entry 3**), suggesting the crucial role of moderate Sn doping. In addition, the poor activity of 1.0 Sn-CeO_2 support verified the critical role of Pt species, which acts as active sites for dehydrogenation (**Table S1, entry 4**). Furthermore, considering the high price of noble metal Pt, relative catalytic performance (mol/mol) was calculated based on the Pt loading amounts to evaluate the utilization of Pt sites (**Fig. 9b and Fig. S3**). It was estimated to be 0.55 mol/mol on 0.1 Pt/1.0 Sn-CeO_2, which was much higher than that on the other *m* Pt/1.0 Sn-CeO_2 catalysts (0.05~0.30 mol/mol). These results revealed that 0.1 Pt/1.0 Sn-CeO_2 could act as efficient catalyst in the selective conversion of propane and CO_2 to propylene.

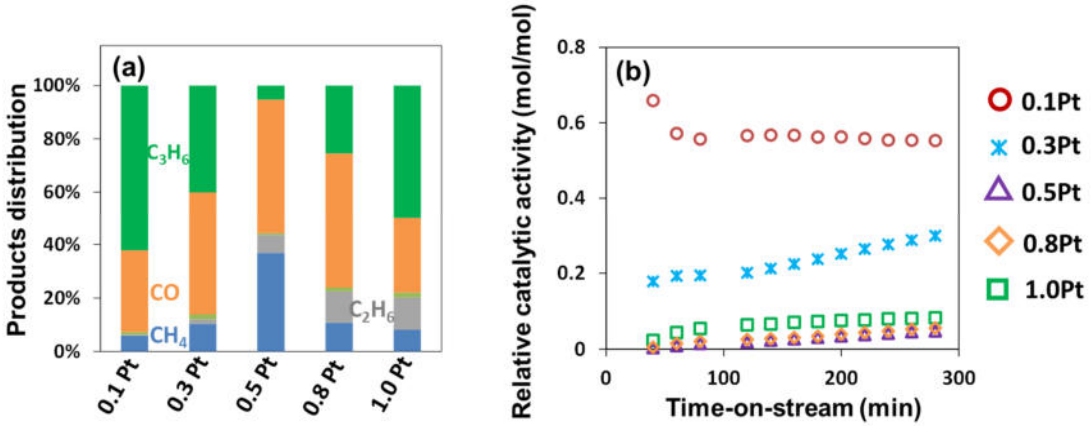

Fig. 9. Catalytic CO_2-ODHP over *m* Pt/1.0 Sn-CeO_2 catalysts with various Pt loading amounts ranging from 0.1 wt% to 1.0 wt%. (a) Products distribution after reaction for 200 min; (b) relative catalytic activity of Pt species (mol/mol), which is calculated from the molar ratio of produced propylene to Pt species.

Typically, the catalysts of 0.1 Pt/1.0 Sn-CeO_2, 0.5 Pt/1.0 Sn-CeO_2, and 1.0 Pt/1.0 Sn-CeO_2 were selected to study the effects of Pt loading amounts on catalytic performances. The elemental mapping results were shown in **Fig. 10**. The Pt species dispersed uniformly when Pt loading amount was lower than 0.5 wt%. Increasing the Pt loading to 1.0 wt%, Pt clusters were observed, indicating the aggregation of Pt species during the reduction. It might be the reason why the propane/CO_2 conversion decreased when the ceria-based catalysts with a high loading amount of Pt species.

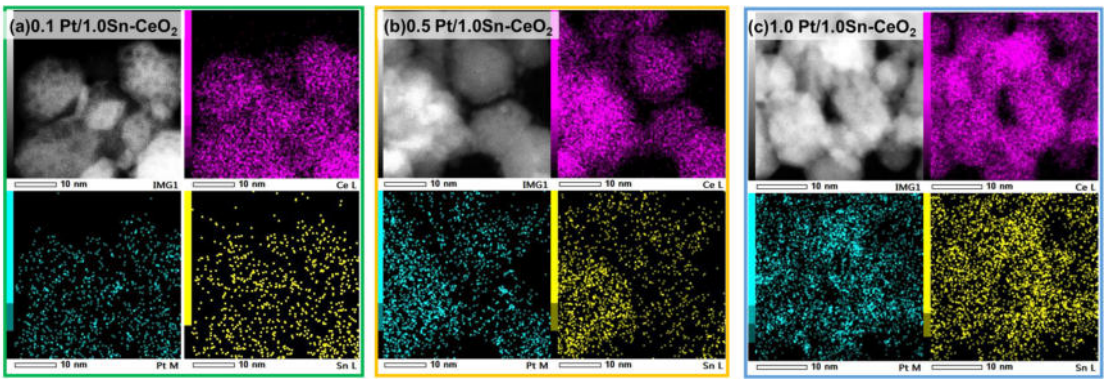

Fig. 10. Elemental mapping results of (a) 0.1 Pt/1.0Sn-CeO_2, (b) 0.5 Pt/1.0Sn-CeO_2, and (c) 1.0 Pt/1.0Sn-CeO_2. Before the detection, these samples were reduced at 450 °C for 1 h in H_2 (25 mL/min).

Effect of Sn doping on the activation of C_3H_8 and CO_2

To better understand the effect of Sn during CO_2-ODHP, the adsorption of propane on the optimized catalyst 0.1 Pt/1.0Sn-CeO_2 along with the control catalyst were tracked by *in situ* FTIR spectroscopy (**Fig. 11**). From the *in situ* IR spectra of both 0.1 Pt/CeO_2 and 0.1 Pt/1.0 Sn-CeO_2, two regions located at 2870-2965cm^{-1} and 1300-1450 cm^{-1} were observed, which could be assigned to the vibration of C–H bond of the adsorbed propane on the surface [46-48]. With propane desorption, the intensity of these bands decreased and completely disappeared after 30 min of desorption on 0.1 Pt/CeO_2. In contrast, they were still observed on 0.1 Pt/1.0 Sn-CeO_2, suggesting a stronger adsorption of propane on Pt/1.0 Sn-CeO_2 than that on 0.1 Pt/CeO_2.

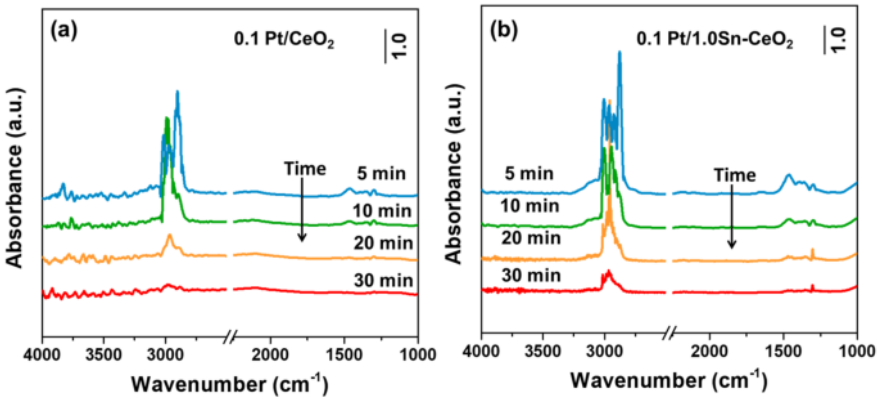

Fig. 11. *In situ IR* spectra for tracking the propane desorption at 550 °C after propane adsorption on catalysts. (a) 0.1 Pt/CeO_2 and (b) 0.1 Pt/1.0 Sn-CeO_2, respectively. Before the propane adsorption, the catalysts were reduced at 450 °C for 30 min.

Then the *in situ* Diffuse Reflectance FTIR was applied to track the propane desorption at various temperatures ranging from 150 °C to 350 °C after propane adsorption at room temperature (**Fig. 12**). The signal associated with adsorbed propane (2965 cm^{-1}) over 0.1 Pt/CeO_2 disappeared completely after desorption at 350 °C, while it was still maintained over 0.1 Pt/1.0 Sn-CeO_2 confirmed the stronger interaction of propane and 0.1 Pt/1.0 Sn-CeO_2. In addition, the intensity of the peak associated with the adsorbed propane on 0.1 Pt/1.0 Sn-CeO_2 was significantly higher than that on 0.1 Pt/CeO_2 under the same conditions, indicating the strong adsorption of propane over the Sn modified catalysts. It was also confirmed by the C_3H_8-TPD, where the peak area

of desorbed propane from 0.1 Pt/1.0 Sn-CeO_2 was significantly increased compared with that on 0.1 Pt/CeO_2 (**Fig. S4**). These results confirmed that the Pt species with rich electrons induced by Sn doping could enhance the adsorption of propane and contribute to the activation of propane.

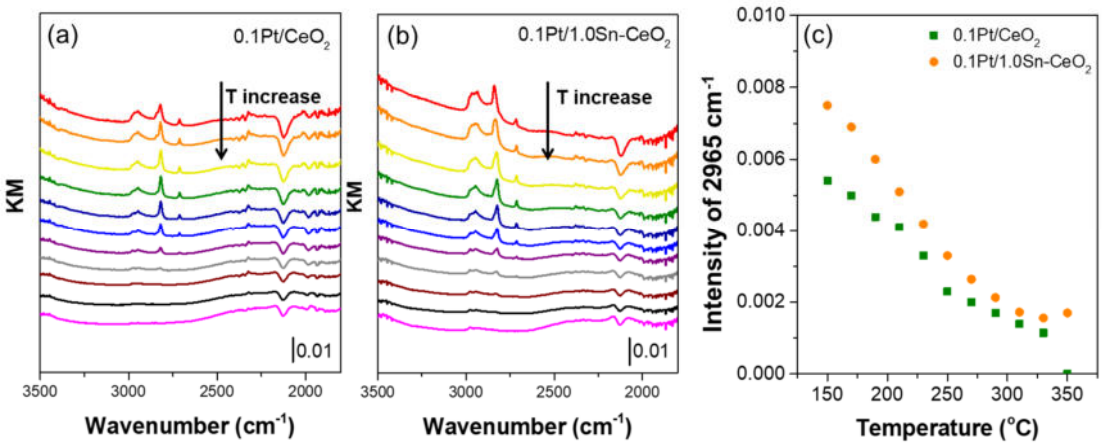

Fig. 12. *In situ* Diffuse Reflectance FTIR of propane desorption at various temperatures ranging from 150 °C to 350 °C after propane adsorption at room temperature over (a) 0.1 Pt/CeO_2, (b) 0.1Pt/1.0Sn-CeO_2, (c) the change of peak intensity located at 2965 cm^{-1} with increasing desorption temperatures. Before the detection, these samples were reduced at 450 °C for 1 h in H_2 (25 mL/min).

The promotion effect of Sn doping on propane activation was also verified by the direct dehydrogenation of propane (**Fig. S5)**. The propane conversion on 0.1 Pt/1.0 Sn-CeO_2 achieved 19%, which was higher than that on 0.1 Pt/CeO_2 (8%) with a similar propylene selectivity (~80%) for both catalysts. It revealed that enhancement of propane adsorption on 0.1 Pt/1.0 Sn-CeO_2 might contribute to the superior catalytic activity in the activation of C–H bonds of propane.

H_2-TPR was conducted to evaluate the donating oxygen abilities of 0.1 Pt/CeO_2 and 0.1 Pt/1.0 Sn-CeO_2, which was crucial for the redox process involved in the CO_2-ODHP reaction (**Fig. 13**). Two reduction peaks located at 478 °C and 792 °C were observed on pristine CeO_2, which could be attributed to the reduction of surface oxygen and bulk oxygen, respectively [33, 34]. After Sn doping, the reduction peak assigned to bulk oxygen showed no obvious change, however, the reduction peak assigned to the

surface oxygen shifted to a lower temperature (348 °C). It was concluded that the introduction of Sn dopant probably led to the formation of SnCe solid solution and activated the surface oxygen of CeO_2-based support, resulting in lowering the reduction temperature [49]. It was also in a good agreement with our previous work [30]. The impregnation of Pt sites on 1.0 Sn-CeO_2 further decreased the reduction temperature of surface oxygen to 223 °C. It might result from the hydrogen spillover between noble metals and reducible metal oxide supports [50, 51]. For comparison, 0.1 Pt/CeO_2 catalyst also showed a shift of reduction peak to lower temperature (from 478 °C to 299 °C) after supporting Pt sites, but it was still much higher than that on 0.1 Pt/1.0 Sn-CeO_2. These results revealed the excellent oxygen releasing capability of 1.0 Sn-CeO_2 support after supporting 0.1 wt% Pt sites. The excellent capability of 0.1 Pt/1.0 Sn-CeO_2 for donating oxygen would promote the formation of oxygen vacancies and make a superiority in a redox process, which was involved in the catalytic CO_2-ODHP reaction.

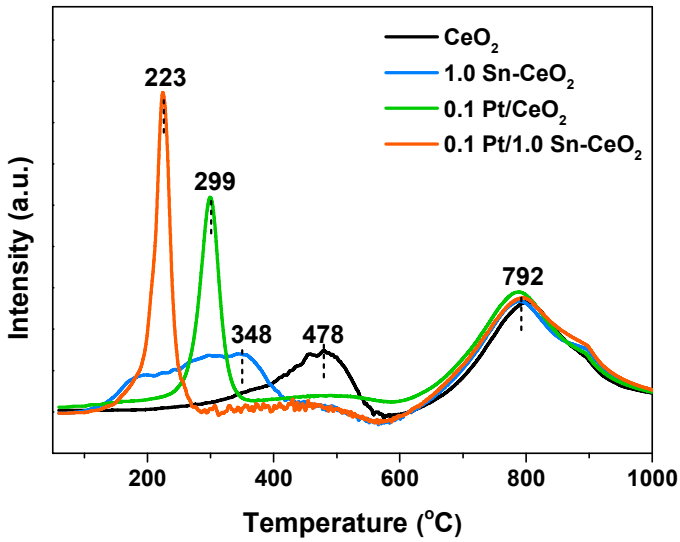

Fig. 13. H_2-TPR results of pristine CeO_2, 1.0 Sn-CeO_2, 0.1 Pt/CeO_2 and 0.1 Pt/1.0 Sn-CeO_2, respectively.

The donating oxygen abilities facilitated the formation of oxygen vacancies on defective CeO_2, which generally acted as active sites for CO_2 dissociation. The

dissociation of CO_2 on defective CeO_2-based catalysts would release CO and active oxygen. Here, CO_2-TPO was conducted to detect the generation of CO via CO_2 dissociation on CeO_2, 1.0 Sn-CeO_2, 0.1 Pt/CeO_2, and 0.1 Pt/1.0 Sn-CeO_2 after reduction (**Fig. 14**). For pristine CeO_2, CO was released at around 434 °C, while it decreased to 412 °C on 1.0 Sn-CeO_2, indicating that Sn doping showed a positive effect on CO_2 dissociation. It further decreased to 317 °C on 0.1 Pt/1.0 Sn-CeO_2, revealing that the oxygen vacancies on defective CeO_2 could be replenished by CO_2 dissociation and this process proceeds easier on 0.1 Pt/1.0 Sn-CeO_2 than that on CeO_2 and 1.0 Sn-CeO_2 as well as 0.1 Pt/CeO_2. In addition, it was noteworthy that the intensity of CO signal (m/z=28) decreased remarkably after the introduction of Pt sites. It suggested that the electron-rich Pt sites were likely anchored on defect sites of Sn-CeO_2 support, partially blocking the CO_2 dissociation. This phenomenon was also observed on CeO_2 support before and after supporting Pt (**Fig. 14 b** and **14 d**).

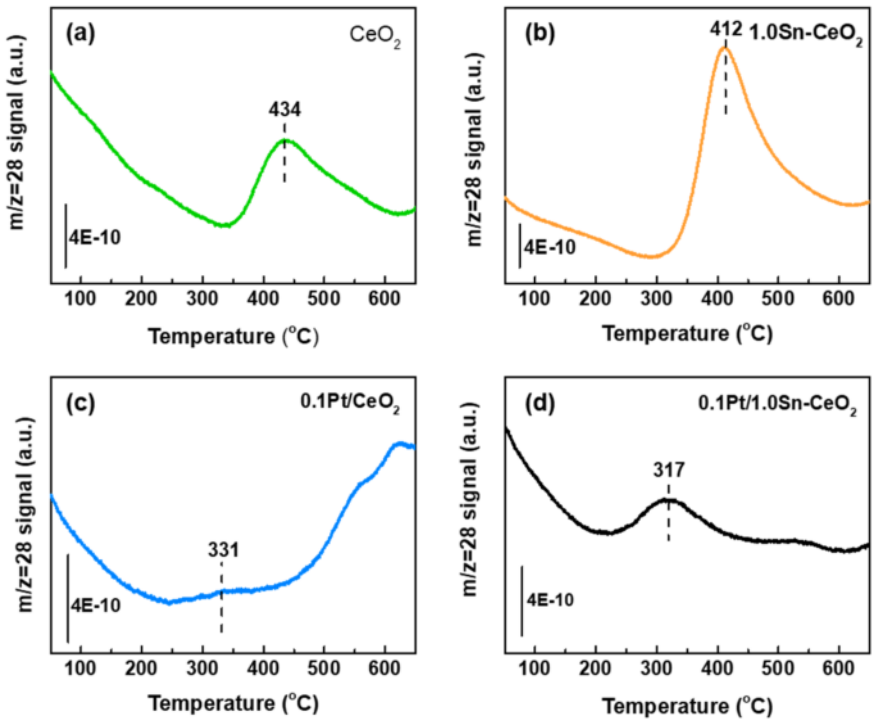

Fig. 14. CO_2-TPO results of (a) pristine CeO_2, (b) 1.0 Sn-CeO_2, (c) 0.1 Pt/CeO_2 and (d) 0.1 Pt/1.0 Sn-CeO_2, respectively. Before detection, the samples were reduced at 450 °C for 30 min in H_2 (10 mL/min).

Proposed reaction mechanism

Finally, the reaction between propane and CO_2 was tracked by *in situ* IR spectroscopy at reaction conditions (**Fig. 15**). After the activation of propane on 0.1 Pt/1.0 Sn-CeO_2, which was verified by the presence of bands at 2870-2965 cm^{-1} and 1300-1450 cm^{-1}, CO_2 was introduced to the reaction system (**Fig. 15a**). The bands located at 2121 cm^{-1} and 2174 cm^{-1} were observed, which could be assigned to the vibration of the released gaseous CO, while another band at around 3600cm^{-1} was assigned to hydroxyl group (–OH) [36, 43, 44] (**Fig. 15 b-c**). During the reaction, the signals attributed to adsorbed propane decreased and then disappeared completely. Meanwhile, the bands associated with –OH and CO increased initially and then decreased with the conversion of propane (**Fig. 15d**). This result suggested that a MvK reaction mechanism was probably involved.

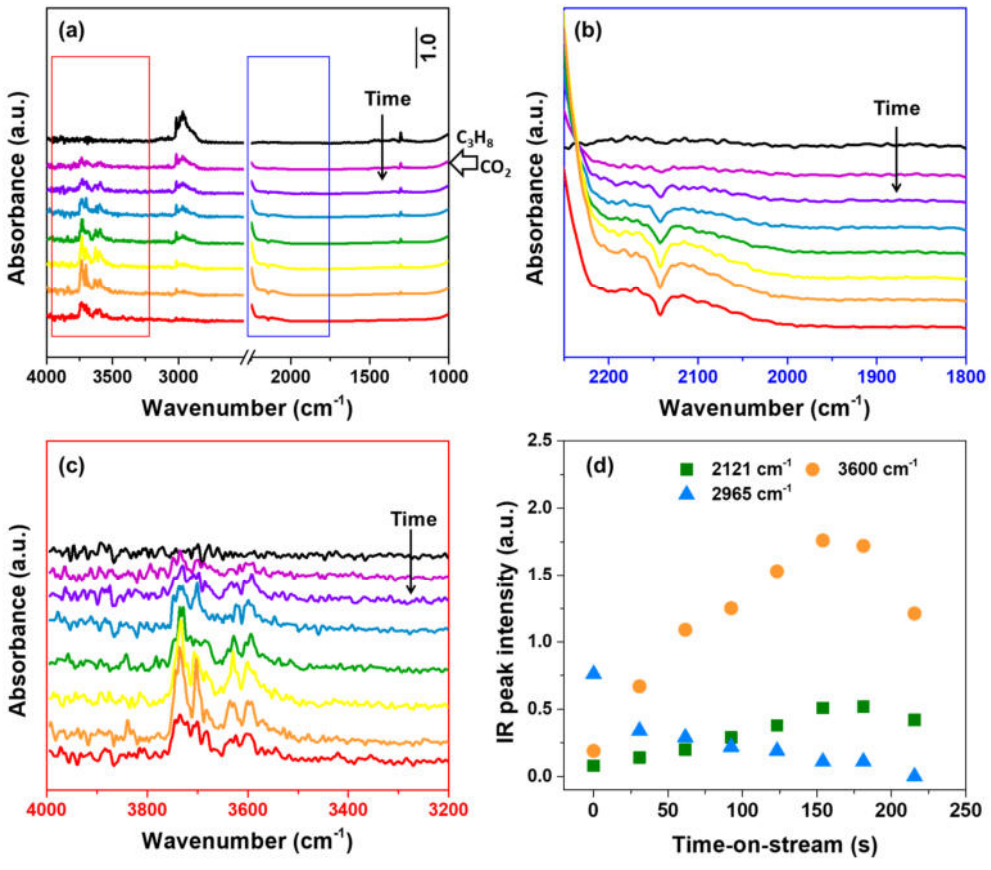

Fig. 15. (a) *In situ* IR spectra of propane and CO_2 adsorption in a stepwise on 0.1 Pt/1.0 Sn-CeO_2 catalysts and then the evolution during the reaction. (b) The *in situ* IR spectra magnified in a range of 2350-1800 cm^{-1}. (c) The *in situ* IR spectra magnified in a range

of 4000-3200 cm^{-1}. (d) The intensity changes of peaks located at 3600, 2965, and 2121 cm^{-1}, respectively, which are associated with the vibration of –OH, C–H, and CO.

On the basis of *in situ* IR results, a MvK reaction mechanism was proposed as follows: 1) propane strongly adsorbed on electron-rich Pt species to release active hydrogen and adsorbed propylene, and the generated active hydrogen transferred to support surface via hydrogen spillover, generating hydroxyl group; 2) Sn-CeO_2 support donated surface oxygen to promote the surface species desorption as water and propylene, leading to the formation of oxygen vacancies simultaneously; 3) CO_2 was dissociated on the oxygen vacancies, generating adsorbed CO and active oxygen species, subsequently replenishing these oxygen vacancies; 4) the generated CO was released and the catalysts returned to the initial states for the next catalytic cycle (**Scheme 2.**).

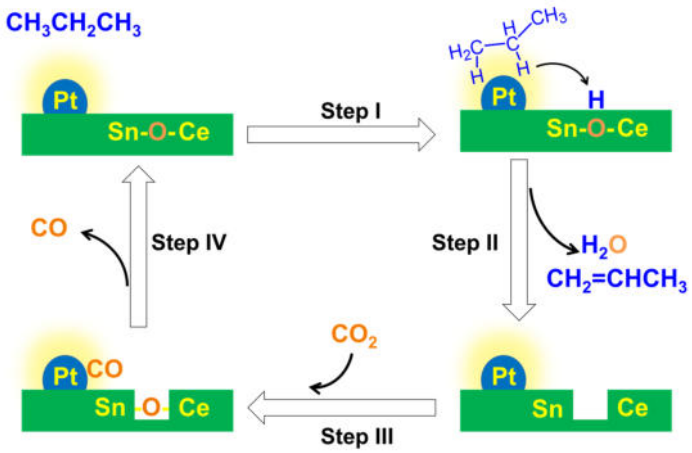

Scheme 2. Proposed reaction mechanism of CO_2-ODHP over Pt/Sn-CeO_2.

Conclusion

In summary, Sn doped CeO_2 supported Pt catalyst was successfully prepared and applied in the CO_2-ODHP. It showed a superiority in the selective production of propylene with a 63.9% selectivity under optimal conditions. A combination of XRD, Raman, H_2-TPR, CO_2-TPD, CO-IR, and *in situ* IR studies suggested that Sn doping

played an essential role in the selective production of propylene. The Sn doping could not only improve the electronic density of Pt species, promoting the propane adsorption and C–H bond cleavage, but also enhance the capability of releasing oxygen, contributing to the dissociation of CO_2. The evolution of propane and CO_2 during the reaction was tracked by *in situ* IR which implied a MvK reaction mechanism. This work not only developed an efficient catalyst for the selective conversion of CO_2 and propane to value-added chemicals, but also provided a comprehensive understanding of the metal doping effects in the catalytic reactions.

Experimental section

Preparation of catalysts

Pristine CeO_2 was prepared by the precipitation method, which was according to the process reported previously [31]. Sn doped CeO_2 (Sn-CeO_2) was prepared by co-precipitation [32, 33]. Typically, a certain amount of $SnCl_4 \cdot 5H_2O$ and Ce $(NO_3)_3 \cdot 6\ H_2O$ were dissolved in 100 mL of water, respectively. 50 mL of ammonia (25 vol%) was added into 50 mL of water to get a solution as the precipitating agent. These three solutions of $SnCl_4$, $Ce(NO_3)_3$, and ammonia were added into a big beaker drop by drop under stirring at room temperature. The generated mixture was filtered and dried at 100 ^oC overnight. At last, a Sn-CeO_2 support was obtained after calcination it at 500 ^oC for 4 h in a muffle furnace. Pt metal was introduced into CeO_2 or Sn-CeO_2 support by wet impregnation method. Typically, a certain volume of H_2PtCl_6 solution (7.692 mM) was dispersed in 10 mL of water, and then 5 g of CeO_2 or Sn-CeO_2 support was added into the H_2PtCl_6 solution under stirring. After stirring for 4 h, the mixture was evaporated at 100 ^oC on a hotplate. At last, CeO_2 or Sn-CeO_2 supported Pt catalysts (denoted as Pt/CeO_2 or Pt/Sn-CeO_2) were obtained by calcination at 550 ^oC in air for 1 h. The Pt/Sn-CeO_2 with various Pt and Sn amounts are denoted as *m* Pt/*n* Sn-CeO_2, where *m*, and *n* represent the percentage loading amount for corresponding metal species.

Characterizations of catalysts

H_2-TPR was conducted on a home-built catalyst characterization system with a mass detector at a heating rate of 10 $^oC \cdot min^{-1}$ with a flow of H_2 (10%)/ Ar. Before the

H_2-TPR detection, the samples were pretreated in Ar (50 mL·min^{-1}) at 550 ºC for 1 h. CO_2-TPO was conducted on an Automated Chemisorption Analyzer (Autochem II 2920, Micromeritics, USA). Before the detection, the catalysts were activated by reduction in H_2 (10 mL/min) at 450 ºC for 30 min. After the reduction, the catalysts were cooled down to room temperature. Then, CO_2 was introduced into the system with a 10 mL/min of feeding speed. The generation of CO (m/z=28) was detected by an online- mass spectrometer. The signal of CO_2 (m/z=44) was also tracked to exclude the CO signal derived from the dissociation of CO_2 itself during the ionization in MS. X-ray photoelectron spectroscopy (XPS) analysis was performed on a Thermofisher Escalab 250 Xi+ (Thermo, USA), equipped with an Al-Kα (1486.6 eV) as the exciting source.

CO-IR spectra were collected from an infrared spectrometer (Tensor 27, Bruker, Germany). The sample was pressed into a self-supporting disk (13 mm in diameter) and placed in a quartz IR cell. Before CO adsorption, the disk was reduced by H_2 (10 mL/min) at 450 ºC for 30 min, and then cooled to room temperature. Then the CO gas was introduced into the sample disk, and maintained for 30 min. The IR spectra of the CO adsorption were recorded after evacuation at room temperature for 30 min. It recorded by 32 scans for per IR spectrum. The *in situ* IR of propane adsorption or step adsorption of propane and CO_2 were conducted at the reaction temperature (550 ºC) for tracking the propane activation and the reaction between CO_2 and propane. Prior to adsorption, the sample disk was also activated by reduction in H_2 (10 mL/min) at 450 ºC for 30 min. Then the propane (2.4 ml/min) or/and CO_2 (4.8 mL/min) were introduced into the system. After adsorption or reaction for 30 min, the corresponding spectra were recorded.

Evaluation of catalytic performances

The catalytic CO_2-ODHP was carried out in a fixed-bed reactor equipped with a vertical quartz tube. 1.0 g of powder catalyst was pressed into pellets and crushed to 40-60 mesh particles. Then they were loaded into the quartz tube and fixed with quartz wools. Before the reaction, the catalyst was activated by reduction in H_2 /N_2 (10 mL/min, and 10 mL/min, respectively) at 450 ºC for 1 h. After the reduction, the H_2

was shut down and the temperature was increased to 550 °C at a heating rate of 2 °C/min with a flow of N_2 (10 mL/min).Then, propane and CO_2 were introduced into the reaction system with a feeding speed of 2.4 mL/min and 4.8 mL/min, respectively. N_2 was applied as the carrier gas (10 mL·min^{-1}). The total gas flow rate is estimated to be 17.2 mL·min^{-1}. Due to the small volume of catalyst loaded (< 0.5 mL) and reaction temperature difference, the mass and heat transport limitation was not be considered in this work. The reaction was conducted at 550 °C except additional instruction. On-line gas chromatography (GC) equipped with TCD and FID detectors was used to analyze the products, including CO, CH_4, and C_2-C_3 hydrocarbons as well as unreacted propane and CO_2. The conversion and selectivity were calculated by the normalization method. The conversion (Equ. (1)-(2)), and selectivity (Equ. (3)-(7)) were defined as follows [34]:

$$\text{Conversion (\%)} = \frac{F(C3H8)_{in} - F(C3H8)_{out}}{F(C3H8)_{in}} \times 100\% \quad (1)$$

$$\text{Conversion (CO2) (\%)} = \frac{F(CO2)_{in} - F(CO2)_{out}}{F(CO2)_{in}} \times 100\% \quad (2)$$

$$\text{Selectivity(C3H6)(\%)} = \frac{F(C3H6)_{out}}{\sum F(C1-C3\ products)_{out}} \times 100\% \quad (3)$$

$$\text{Selectivity (CO)(\%)} = \frac{F(CO)_{out,1} - F(CO)_{out,2}}{\sum F(C1-C3\ products)_{\text{out}}} \times 100\% \quad (4)$$

$$\text{Selectivity(CH4) (\%)} = \frac{F(CH4)_{out}}{\sum F(C1\text{-}C3\ products)_{out}} \times 100\% \quad (5)$$

$$\text{Selectivity (C2H4)(\%)} = \frac{F(C2H4)_{out}}{\sum F(C1-C3\ products)_{out}} \times 100\% \quad (6)$$

$$\text{Selectivity (C2H6)(\%)} = \frac{F(C2H6)_{out}}{\sum F(C1-C3\ products)_{out}} \times 100\% \quad (7)$$

Where, $F(C3H8)_{in}$ is the flow of propane into the reactor; $F(C3H8)_{out}$ is the flow of propane out of the reactor; $F(CO2)_{in}$ is the flow of CO_2 into the reactor; $F(CO2)_{out}$ is the flow of CO_2 out of the reactor; the CO selectivity here was defined to estimate the proceeding of dry reforming reaction; it was noteworthy that when the CO selectivity was calculated, the CO generated via CO_2-ODHP has been deducted. $F(CO)_{out,1}$ is the flow of carbon in all CO out of reactor; $F(CO)_{out,2}$ is the flow of carbon in CO out of reactor via CO_2-ODHP which calculated based on the flow of propylene; $F(CH4)_{out}$, $F(C2H4)_{out}$, or $F(C2H6)_{out}$ is the flow of carbon in CH_4, C_2H_4, C_2H_6 out of reactor,

respectively; $F(C1\text{-}C3\ products)_{out}$ is the flow of all carbon from products out of reactor.

Supporting Information

Supplementary catalyst characterizations such as XRD, C_3H_8-TPD and additional reaction results.

Acknowledgement

This work was supported by the Ministry of Science and Technology of the People's Republic of China (2018YFE0117300), the National Natural Science Foundation of China (22078312, 22172162, 21972139, 22025206, 21991090, 21721004, 22172158), the Dalian Innovation Support Plan for High Level Talents (2020RT10), the Youth Innovation Promotion Association (YIPA) of the Chinese Academy of Sciences (2019185), the Sino-German Mobility Program (M0304). We thank the instrumental support of the Liaoning Key Laboratory of Biomass Conversion for Energy and Material.

Key words:

CeO_2-based catalysts; CO_2 conversion; dehydrogenation of propane; Sn doping

Author contributions

Yehong Wang: Investigation, Formal analysis, Writing-original draft, Writing-review & editing. Jiapei Wang: Investigation, Formal analysis, Writing-review & editing. Yuda Zhang: Investigation, Formal analysis. Qiang Guo: Investigation, Formal analysis. Yafei liang: Investigation, Formal analysis. Jie An: Investigation, Formal analysis. Yafei liang: Investigation, Formal analysis. Yanan Wang: Investigation, Formal analysis. Pengfei Cao: Investigation, Formal analysis. Marc Heggen: Methodology, Funding acquisition. Rafal E. Dunin-Borkowski: Conceptualization, Methodology, Project administration. Xiangxue Zhu: Methodology, Writing-original draft, Writing-review & editing, Funding acquisition. Xiujie Li: Conceptualization, Methodology, Writing-original draft, Writing-review & editing, Funding acquisition, Project administration.

Feng Wang: Conceptualization, Methodology, Funding acquisition, Project administration.

Reference

[1] X. Jiang, L. Sharma, V. Fung, S. J. Park, C. W. Jones, B. G. Sumpter, J. Baltrusaitis, Z. L. Wu, *ACS Catal.*, **2021**, *11*, 2182-2234.

[2] J. J. H. B. Sattler, J. Ruiz-Martinez, E. Santillan-Jimenez, B. M. Weckhuysen, *Chem. Rev.*, **2014**, *114*, 10613-10653.

[3] M. B. Ansari, S. E. Park, *Energy Environ. Sci.*, **2012**, *5*, 9419-9437.

[4] R. You, X. Y. Zhang, L. F. Luo, Y. Pan, H. B. Pan, J. Z. Yang, L. H. Wu, X. S. Zheng, Y. K. Jin, W. X. Huang, *J. Catal.*, **2017**, *348*, 189-199.

[5] K. M. Du, M. J. Hao, Z. N. Li, W. Hong, J. J. Liu, L. P. Xiao, S. H. Zou, H. Kobayashi, J. Fan, *Chin. J. Catal.*, **2019**, *40*, 1057-1062.

[6] M. A. Atanga, F. Rezaei, A. Jawad, M. Fitch, A. A. Rownaghi, *Appl. Catal. B-Environ.*, **2018**, *220*, 429-445.

[7] E. Gomez, B. H. Yan, S. Kattel, J. G. G. Chen, *Nat. Rev. Chem*., **2019**, *3*, 638-649.

[8] A. Alvarez, M. Borges, J. J. Corral-Perez, J. G. Olcina, L. J. Hu, D. Cornu, R. Huang, D. Stoian, A. Urakawa, *ChemPhysChem*, **2017**, *18*, 3135-3141.

[9] F. L. Xing, Y. Nakaya, S. Yasumura, K. Shimizu, S. Furukawa, *Nat. Catal.*, **2022**, *5*, 55-65.

[10] R. Ryoo, J. Kim, C. Jo, S. W. Han, J. C. Kim, H. Park, J. Han, H. S. Shin, J. W. Shin, *Nature*, **2020**, *585*, 221-224.

[11] G. D. Sun, Z. J. Zhao, R. T. Mu, S. J. Zha, L. L. Li, S. Chen, K. T. Zang, J. Luo, Z. L. Li, S. C. Purdy, A. J. Kropf, J. T. Miller, L. Zeng, J. L. Gong, *Nat. Commun.*, **2018**, *9*, 4454.

[12] Z. Wang, Y. Z. Chen, S. J. Mao, K. J. Wu, K. C. Zhang, Q. C. Li, Y. Wang, *Adv. Sustain. Syst.*, **2020**, *4*, 2000092.

[13] J. Wu, Z. M. Peng, A. T. Bell, *J. Catal.*, **2014**, *311*, 161-168.

[14] G. J. Siri, J. M. Ramallo-Lopez, M. L. Casella, J. L. G. Fierro, F. G. Requejo, O. A. Ferretti, *Appl. Catal. A-Gen.*, **2005**, *278*, 239-249.

[15] E. Nowicka, C. Reece, S. M. Althahban, K. M. H. Mohammed, S. A. Kondrat, D. J. Morgan, Q. He, D. J. Willock, S. Golunski, C. J. Kiely, G. J. Hutchings, *ACS Catal.*, **2018**, *8*, 3454-3468.

[16] A. Parastaev, V. Muravev, E. H. Osta, A. J. F. Van Hoof, T. F. Kimpel, N. Kosinov, E. J. M. Hensen, *Nat. Catal.,* **2020**, *3*, 526-533.

[17] K. Tomishige, Y. Gu, T. Chang, M. Tamura, Y. Nakagawa, *Mater. Today Sustain.*, **2020**, *9*, 100035.

[18] L. J. Lei, Y. H. Wang, Z. X. Zhang, J. H. An, F. Wang, *ACS Catal.*, **2020**, *10*, 8788-8814.

[19] Z. Y. Liu, F. Zhang, N. Rui, X. Li, L. L. Lin, L. E. Betancourt, D. Su, W. Q. Xu, J. J. Cen, K. Attenkofer, H. Idriss, J. A. Rodriguez, S. D. Senanayake, *ACS Catal.*, **2019**, *9*, 3349-3359.

[20] E. Gomez, Z. H. Xie, J. G. G. Chen, *AIChE J.*, **2019**, *65*, e16670.

[21] F. Wang, M.Wei, D. G. Evans, X. Duan, *J. Mater. Chem. A*, **2016**, *4*, 5773-5783.

[22] J. J. Liu, M. J. Hao, C. L. Chen, K. M. Du, Q. Y. Zhou, S. H. Zou, L. P. Xiao, J. Fan, *Appl. Surf. Sci.*, **2020**, *528*, 147025.

[23] T. Montini, M. Melchionna, M. Monai, P. Fornasiero, *Chem. Rev.*, **201**6, *116*, 5987-6041.

[24] H. F. Xiong, S. Lin, J. Goetze, P. Pletcher, H. Guo, L. Kovarik, K. Artyushkova, B. M. Weckhuysen, A. K. Datye, *Angew. Chem. Int. Ed.*, **2017**, *56*, 8986–8991.

[25] C. L. Yu, Q. J. Ge, H. Y. Xu, W. Z. Li, *Appl. Catal. A-Gen.*, **2006**, *315*, 58–67.

[26] L. Wang, G. Q. Yang, X. Ren, Z. W. Liu, *Nanomaterials,* **2022**, *12*, 417,

[27] Z. X. Zhang, Y. H. Wang, J. M. Lu, J. Zhang, M. R. Li, X. B. Liu, F. Wang, *ACS Catal.*, **2018**, *8*, 2635-2644.

[28] Z. X. Zhang, Y. H. Wang, J. M. Lu, C. F. Zhang, M. Wang, M. R. Li, X. B. Liu, F. Wang, *ACS Cata*l., **2016**, *6*, 8248-8254.

[29] H. D. Wang, G. Tsilomelekis, *Catal. Sci. Technol.*, **2020**, *10*, 4362-4372.

[30] Y. H. Wang, M. Peng, J. Zhang, Z. X. Zhang, J. H. An, S. Y. Du, H. Y. An, F. T. Fan, X. Liu, P. Zhai, D. Ma, F. Wang, *Nat. Commun.*, **2018**, *9*, 5183.

[31] Y. H. Wang, F. Wang, Q. Song, Q. Xin, S. T. Xu, J. Xu, *J. Am. Chem. Soc.*, **2013**,

135, 1506-1515.

[32] J. F. Liu, W. Zhou, D. Y. Jiang, D. Wang, W. H. Wu, Y. Wang, X. B. Ma, *Catal. Today*, **2021**, *368*, 58-65.

[33] P. Venkataswamy, K. N. Rao, D. Jampaiah, B. M. Reddy, *Appl. Catal. B-Environ.*, **2015**, *162*, 122-132.

[34] Y. H. Wang, Z. X. Zhang, L. J. Lei, W. Liu, S. Y. Du, X. X. Zhu, X. J. Li, F. Wang, *ACS Sustain. Chem. Eng.*, **2021**, *9*, 17301-17309.

[35] E. Gomez, S. Kattel, B. H. Yan, S. Y. Yao, P. Liu,; J. G. G. Chen, *Nat. Commun.*, **2018**, *9*, 1398.

[36] X. I. Pcrcira-Hcrnandcz, A. Delariva, V. Muravev, D. Kunwar, H. Xiong, B. Sudduth, M. Engelhard, L. Kovarlk, E. J. M. Hcnscn, Y. Wang, A. K. Datye, *Nat. Commun*., **2019**, *10*, 1358.

[37] R. Burch, *J. Catal.*, **1981**, *71*, 348-359.

[38] C. Larese, J.M. Campos-Martin, J.J. Calvino, G. Blanco, J.L.G. Fierro, Z.C. Kang, *J. Catal.*, **2002**, *208*, 467-478.

[39] K. Ding, A. Gulec, A. M. Johnson, N. M. Schweitzer, G. D. Stucky, L. D. Marks, P. C. Stair, *Science*, **2015**, *350*, 189-192.

[40] G. J. Kim, D. W. Kwon, S. C. Hong, *J. Phys. Chem. C*, **2016**, *120*, 17996-18004.

[41] J. S. Xu, C. X. Shi, S. G. Zhang, Q. C. Zheng, L. Pan, X. W. Zhang, J. J. Zou, *Chin. J. Chem* . **2022**, *40*, 918-924.

[42] Y. C. Pei, Z. Y. Qi, T. W. Goh, L. L. Wang, R. V. Maligal-Ganesh, H. L. Macmurdo, S. R. Zhang, C. X. Xiao, X. L. Li, F. Tao, D. D. Johnson, W. Y. Huang, *J. Catal.*, **2017**, *356*, 307-314.

[43] A. M. D. De Farias, D. Nguyen-Thanh, M. A. Fraga, *Appl. Catal. B-Environ.*, **2010**, *93*, 250-258.

[44] M. Guo, J. Q. Lu, Y. N. Wu, Y. J. Wang, M. F. Luo, *Langmuir*, **2011**, *27*, 3872-3877.

[45] S. Loridant, *Catal. Today*, **2021**, *373*, 98-111.

[46] B. Wang, X. D. Wu, R. Ran, Z. C. Si, D. Weng, *J. Mol. Catal. A-Chem.*, **2012**, *356*, 100-105.

[47] M. A. Hasan, M. I. Zaki, L. Pasupulety, *J. Phys. Chem. B*, **2002**, *106*, 12747-12756.

[48] W. L. S. Faria, C. A. C. Perez, D. V. Cesar, L. C. Dieguez, M. Schmal, *Appl. Catal. B-Environ.*, **2009**, *92*, 217-224.

[49] T. Y. Deng, H. C. Liu, *Green Chem.*, **2013**, *15*, 116-124.

[50] R. Prins, *Chem. Rev.*, **2012**, *112*, 2714-2738.

[51] M. M. Bettahar, *Catal. Rev.*, **2022**, *64*, 87-125.

TOC:

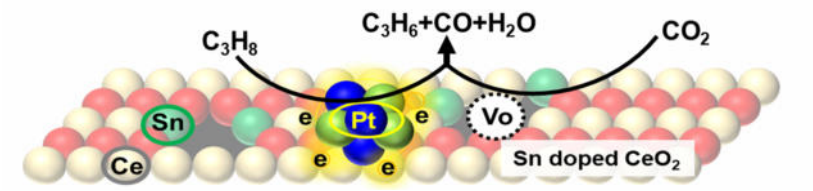

A Pt/Sn-CeO_2 catalyst shows a higher catalytic activity in CO_2-ODHP than a Pt/ CeO_2 catalyst. It derives from the crucial role of Sn dopant. The Sn doping not only increases the electron density of Pt species via PtSn alloy formation but also enhances oxygen vacancy concentrations of CeO_2 support, leading to the enhancement of propane adsorption and CO_2 dissociation.

Characterizations of catalysts

Powder X-ray diffraction patterns (XRD) was conducted on a PANalytical X-Pert PRO diffractometer, using Cu-Ka radiation at 40 kV and 20 mA. Continuous scans were collected in the 2θ ranging from 10 ° to 75°, at a step rate of 10°·min^{-1}. Raman spectra were collected with a 532 nm constant-wave laser (Senterra, Bruker, Germany) served as the excitation source. C_3H_8-TPD was performed on a Micromeritics Autochem 2920 instrument. About 0.2 g of the sample was pre-reduced at 450 ºC for 1 h in 5 vol% H_2 /Ar. After this, the sample was cooled to 70 ºC and purged with Ar. Then, the pre-treated sample was saturated with pure C_3H_8 with a flow rate of 30 mL/min for 1 h. Then, the sample was purged by an Ar stream for 1 h, and temperature-programmed desorption of C_3H_8 was performed from 70 to 600 ºC at a heating rate of 10 ºC/min. The amount of desorbed C_3H_8 was monitored and determined by a pre-calibrated thermal conductivity detector (TCD).

Figures and tables

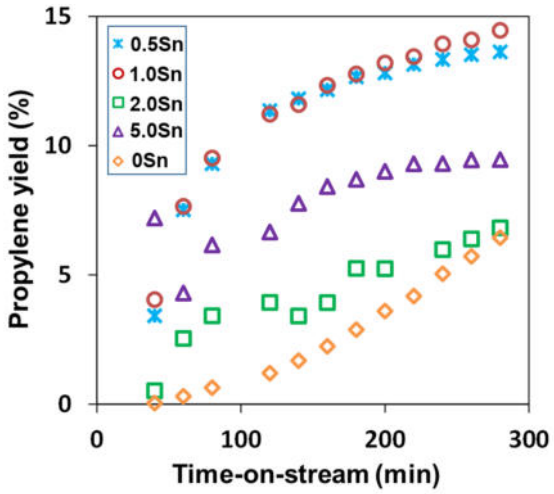

Fig. S1. Propylene yield over 1.0 Pt/CeO_2 and 1.0 Pt/*n* Sn-CeO_2 with various Sn doping amounts ranging from 0.5 wt% to 5 wt% in CO_2-ODHP reaction.

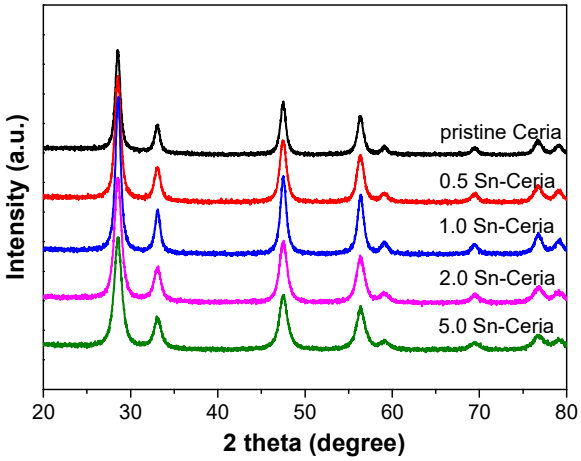

Fig. S2. XRD patterns of pristine CeO_2 and various Sn doped CeO_2.

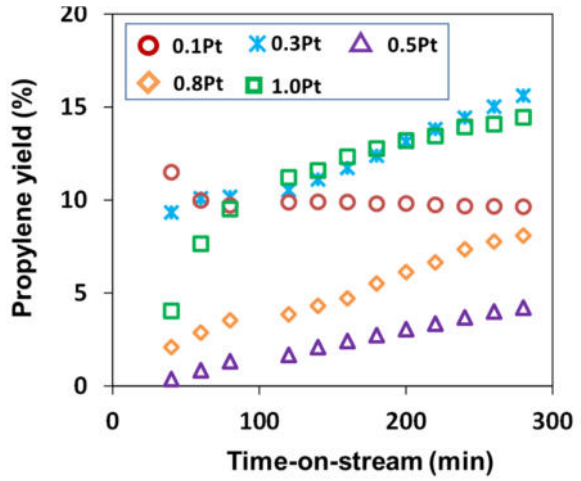

Fig. S3. Propylene yield over *m* Pt/1.0 Sn-CeO_2 with various Pt loading amounts ranging from 0.1 wt% to 1.0 wt% in CO_2-ODHP reaction.

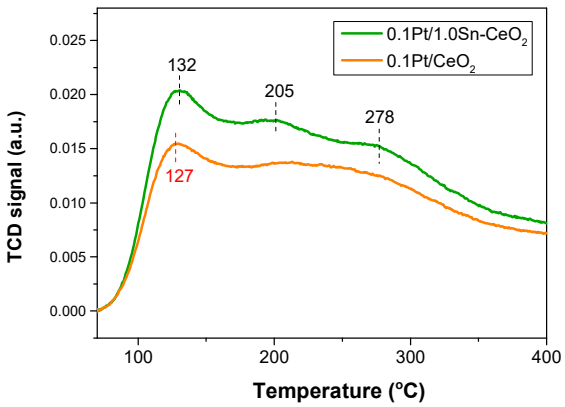

Fig. S4. The C_3H_8-TPD results of 0.1Pt/CeO_2 and 0.1 Pt/1.0 Sn-CeO_2.

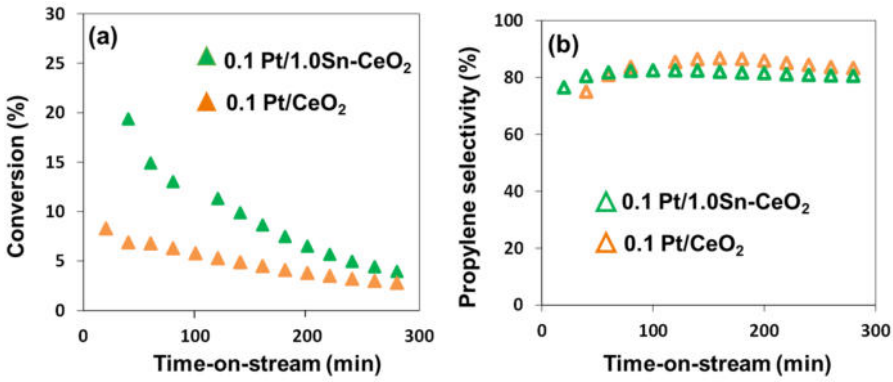

Fig. S5. Catalytic direct dehydrogenation of propane over 0.1 Pt/CeO_2 and 0.1 Pt/1.0 $Sn-CeO_2$, respectively. (a) Conversion of propane; (b) propylene selectivity. Reaction conditions: catalysts, 1.0 g, 40-60 mesh; the feeding speed of propane is 2.4 mL/min; the reactions were conducted at 550 ºC with N_2 as carrier gas (10 mL/min); before the reaction, the catalysts were pretreated in H_2 (10 mL/min) at 450 ºC for 1 h.

Table S1. Catalytic performances of various catalysts.

Entry	Catalyst	Conversion (%)	Selectivity (%)
1	-	<2	--
2	0.1 Pt/1.0 $Sn-CeO_2$	15.1	63.9
3	0.1 Pt/CeO_2	14.3	22.3
4	1.0 $Sn-CeO_2$	7.1[a]	31.0[a]

Reaction conditions: catalysts, 1.0 g, 40-60 mesh; the feeding speed of propane and CO_2 is 2.4 mL/min and 4.8 mL/min, respectively; these reactions were conducted at 550 ºC for 240 min with N_2 as carrier gas (10 mL/min); before the reaction, these catalysts were pretreated in H_2 (10 mL/min) at 450 ºC for 1 h; [a] 100 min.